Stochastic wall model for turbulent pipe flow using Immersed Boundary Method and Large Eddy Simulation

Hanane Atmani, Rémi Zamansky, Eric Climent, Dominique Legendre

Version of Record: https://www.sciencedirect.com/science/article/pii/S0045793022000834
Manuscript_0348f6250eab679bef90ca57820a39e0

Stochastic wall model for turbulent pipe flow using Immersed Boundary Method and Large Eddy Simulation

Hanane Atmani, Rémi Zamansky, Eric Climent, Dominique Legendre

Institut de Mécanique des Fluides de Toulouse (IMFT), Université de Toulouse, CNRS

2 Allée du Professeur Camille Soula, Toulouse, 31400, France.

corresponding author: dominique.legendre@imft.fr

Keywords: Turbulent pipe flow, Immersed Boundary Method (IBM), Large Eddy Simulation (LES), stochastic wall model

Abstract

A hybrid IBM-LES method is presented with the objective to simulate high-Reynolds number pipe flows on coarse Cartesian meshes. The IBM method is first used to simulate a laminar pipe flow and results have shown to converge with second order accuracy to the exact solution. A new forcing scheme inside the IBM wall thickness improves significantly numerical accuracy and provides an interesting way to control the fluid-solid interaction. Based on this new modeling of the IBM wall boundary condition, turbulent pipe flows for Reynolds numbers in the range 50,000 to 500,000 are then considered. The IBM wall forcing under these conditions is developed based on the classical turbulent wall laws, namely the log-law and the power-law, able to reproduce the mean velocity profile. We show that adjusting the control parameters of these two models makes possible to recover the correct bulk velocity and mean velocity profile. In order to improve the fluctuations level and spatial distribution of turbulent structures inside the pipe, we propose to extend the log-law modeling using local and unsteady value of the wall shear stress obtained from a stochastic model. The latter preserves spatiotemporal correlations of the wall friction and enhances the reliability of the simulations in terms of both mean bulk flow and fluctuations. The effects of both the Reynolds number and the grid resolution are also discussed and empiric correlations for the model parameters are proposed.

1 Introduction

Most flows present both in nature and in industrial applications are often characterized by a high Reynolds number resulting in a turbulent regime. A precise description both in time and space of such flows requires Direct Numerical Simulation (DNS) which consists in solving the whole range of temporal and spatial scales. To do, realistic configurations are highly demanding in terms of computational resources which are in most of the cases beyond the actual capacity of even the most powerful supercomputers. To overcome this limitation, two common methods are used: Reynolds Averaged Navier-Stokes (RANS) equations and Large Eddy Simulation (LES). While the former is based on a space and/or time averages yielding drastic reduction of the accuracy, LES, on the other hand, resolves the large scales thanks to an appropriate modeling of small scale (unresolved) dynamics and is able to provide results closer to DNS [1].

The filtering procedure of the Navier-Stokes equations, leads to the occurrence of new unknowns (sub-grid tensor) in the LES equations which need to be modeled. Different methods have been proposed [2] such as constant Smagorinsky model, dynamic Smagorinsky model, Bardina model, Chollet-Lesieur model, WALE ... The choice of the adequate method depends mainly on the flow conditions. One of the most serious issues of the applicability of LES for wall bounded flows at large Reynolds numbers is that the number of mesh points becomes prohibitively large if one intends to resolve the near-wall layer [3]. On the other hand, the use of wall models to circumvent this problem and use larger cells close to the walls has been proposed for a long time. Nevertheless, even with such wall models, generating meshes that fit the boundary is often complex and still requires a significant number of grid points.

In addition, turbulent flows in applications often occur in complex geometries. The Immersed Boundary Method (IBM) has been proved to be an efficient and practical approach to simulate the presence of solids on a simple regular mesh regardless of the complexity of the geometry. This method was first introduced by Peskin [4] to study flow patterns around heart valves and has evolved over the years into a general framework for fluid/structure interactions. Inspired by the work of Peskin, many approaches were developed afterwards. Generally, we refer to two major types of IBM: sharp IBM, in which the solid boundary is located within one cell and diffuse IBM, as used in this study, providing a smooth transition between the fluid and the solid across three to four cells. When simulating a moving IB solid using sharp IBM, it is possible to experience some spurious oscillations because of the sharp variation of the nature of some cells going from being solid cells to fluid cells or vice versa. This change may produce spatial discontinuity in the pressure across the IB boundary caused by the new fluid cells or a temporal discontinuity in the velocity at the solid cells [5]. With diffusive IBM, the IBM thickness provides a smooth evolution of the IBM force and thus is less sensitive to the numerical oscillations.

Simulating turbulent flows by coupling IBM for the complex geometry and LES for turbulence also raises the question of adapting the wall boundary conditions for their coupling. The resolved LES can capture the viscous boundary layer therefore requires an adapted mesh refinement close to the wall. Specific wall conditions for IBM walls to overcome that resolution constraint were proposed. Tessicini et al. [6] solved the LES equations up to the second grid cell away from the wall, then switched to solving the simplified turbulent boundary-layer equations on an embedded refined wall mesh. The eddy viscosity is obtained from a simple blend of an eddy viscosity model with near wall damping function. Cristallo & Verzicco [7] have upgraded the work of Tessini et al. [6] by using LES from the bulk flow to the nearest grid point at the wall while the wall shear stress is deduced from a boundary layer approximation. Roman et al. [8] used a prediction of the velocity at the first fluid grid point in contact with the IB solid boundary assuming the classical log-law evolution and imposed a RANS-like eddy viscosity elsewhere. We note that these methods have been developed in the context of sharp immersed boundaries when the wall is well located on the Eulerian grid. Using a diffuse IBM with Lagrangian markers, Ma et al. [9] solved the boundary layer equations on an embedded mesh and used the local wall shear stress calculated from Eulerian points to correct the sub-grid scale viscosity.

In the present paper, we propose a combination of wall models for Large Eddy Simulation and diffuse Immersed Boundary Method to address high Reynolds numbers pipe flow that has received little attention for CFD investigation due to numerical method limitations. We propose the use a uniform mesh with a particularly coarse resolution thanks to an IBM and LES coupling allowing nevertheless to obtain quite a satisfactory resolution of the flow despite the very high Reynolds numbers considered. For the purpose of model validation in such condition, we consider the configuration of turbulent pipe flow which has been investigated in some experiments. For instance, Laufer [10] measured the flow statistics for $Re = 50,000$ and $Re = 500,000$. The Superpipe facility in Princeton served for many experimental studies over a wide range of Reynolds numbers: Zagarola & Smit [11] provided the mean velocity profiles and Hultmark et al. [12] reported on the RMS of streamwise velocity fluctuations and discussed the scaling of the velocity as well as the location of the fluctuation peak. Meanwhile, numerical simulations were also carried out for high Reynolds numbers. Chin [13] provided information on the mean flow velocity and RMS fluctuations

for a pipe at Reynolds number Re up to $83,000$ using DNS and Vijiapurapu & Cui [14] compared the mean velocity profile obtained from LES and RANS for $Re = 100,000$.
Thus, the main objective of our work is to couple IBM and LES solvers to make possible the simulation of large Reynolds number turbulent pipe flows on coarse Cartesian meshes. Section 2 introduces the numerical methods for IBM, LES and their coupling. In section 3, a Poiseuille flow is simulated for different meshes and serves as a proof of concept for the proposed approach to model the solid-fluid interaction. In section 4, high Reynolds number turbulent pipe flows are considered and a new model coupling the classical wall law and a stochastic approach is proposed and validated with previous existing data.

2 Numerical methods and set-up

As explained in the introduction, the main objective of this work is to couple IBM and LES methods through a wall model to simulate high Reynolds number turbulent flows. The numerical development and the CFD simulations are carried out using the IMFT in-house code JADIM, the latter is based on a 3D unsteady incompressible Navier-Stokes equation solver for Newtonian fluids [15, 16]. In this section, we rapidly introduce the IBM and LES solvers and present the numerical strategy proposed and validated in the current work.

2.1 Governing equations

We consider the 3D unsteady incompressible Navier-Stokes system of equations for a Newtonian fluid in Cartesian coordinates:

$$\frac{\partial u_i}{\partial x_i} = 0 \tag{1}$$

$$\frac{\partial u_i}{\partial t} + \frac{\partial u_i u_j}{\partial x_j} = -\frac{1}{\rho}\frac{\partial p}{\partial x_i} + \nu \frac{\partial^2 u_i}{\partial x_i \partial x_j} + f_i \tag{2}$$

where u_i ($i = 1, 2, 3$) is the velocity field, p is the pressure field and f_i stands for any volumetric combination of forces applied to the fluid. ρ, μ and $\nu = \mu/\rho$ are the fluid density, dynamic viscosity and kinematic viscosity, respectively. The discretization is achieved using the finite volume method. The time integration is done using Runge-Kutta 3 (RK3) scheme and the diffusive viscous terms are solved by a semi-implicit Crank-Nicolson (CN) scheme [15].

The IBM solver
The IBM approach developed for simulating the solid-fluid interaction is detailed in [17]. The method is summarized here considering a fixed solid object. It is based on the definition of a "solid volume fraction" α_{IBM}, which is equal to 1 in cells filled with the solid phase, 0 in cells filled with the fluid phase, and $0 < \alpha_{IBM} < 1$ in the region of the diffuse boundary. The solid fluid interaction is represented by a forcing term added to Navier-Stokes equations as a contribution to the volumetric force f:

$$f_{IBM} = \alpha_{IBM} \frac{v_s - \widehat{u}}{\Delta t} \tag{3}$$

where Δt is the time step used for time advancement, v_s is the local velocity imposed to the immersed solid object and $\widehat{u}$ is a predictor velocity without considering the immersed object.

The overall algorithm is as follows. Starting from the divergence-free velocity field u_i^n at time n and the pressure field $p^{n-1/2}$ at time $n - 1/2$, a mixed RK3-CN loop ($k = 1, 2, 3$) is applied with $\widehat{u}_i^0 = u_i^n$. The intermediate velocity field $\widehat{u}_i^k$ is first computed without considering fluid-solid interaction:

$$\frac{\widehat{u}_i^k - \widehat{u}_i^{k-1}}{\Delta t} = SM_i^k \tag{4}$$

with

$$\begin{aligned} SM_i^k &= \gamma_k N(\widehat{u}_i^{k-1}) + \xi_k N(\widehat{u}_i^{k-2}) + (\alpha_k + \beta_k) L(\widehat{u}_i^{k-1}) \\ &+ (\alpha_k + \beta_k)[f_i - \frac{1}{\rho^{n+1/2}} \nabla p^{n-1/2}] \end{aligned} \tag{5}$$

where α_k,β_k, γ_k, ξ_k are the Runge-Kutta coefficients. N (resp. L) is a non-linear (resp. linear) operator containing the advective and viscous terms.

The IBM fluid-coupling term f_{IBM} defined by (3) is then computed as:

$$f_{IBM,i}^k = \alpha_{IBM} \frac{v_{s,i}^{k-1} - \widehat{u}_i^k}{\Delta t} \tag{6}$$

In practice, the transition region $0 < \alpha_{IBM} < 1$ has to fit within one-to-three grid cells [18]. Note that when the solid is fixed, $v_{s,i}^{k-1}$ is set to 0 inside the transition region and the IBM coupling term f_{IBM}^k is thus simplified to:

$$f_{IBM,i}^k = -\alpha_{IBM} \frac{\widehat{u}_i^k}{\Delta t} \tag{7}$$

The intermediate velocity field including the solid-fluid interaction is then computed as:

$$\frac{\widehat{u}_i^k - \widehat{u}_i^{k-1}}{\Delta t} = \beta_k L(\widehat{u}_i^k - \widehat{u}_i^{k-1}) + SM_i^k + f_{IBM,i}^k \tag{8}$$

At the end of the RK3 loop, the velocity $\tilde{u}_i^{n+1} = \widehat{u}_i^3$ is not divergence free and the projection method is applied. The auxiliary potential Φ^{n+1} is obtained by solving the Poisson equation:

$$\frac{\partial^2 \Phi^{n+1}}{\partial x_i \partial x_i} = \frac{\rho}{\Delta t} \frac{\partial \tilde{u}_i^{n+1}}{\partial x_i} \tag{9}$$

and the final pressure and divergence-free velocity are obtained:

$$p^{n+\frac{1}{2}} = p^{n-\frac{1}{2}} + \Phi^{n+1} \tag{10}$$

$$u_i^{n+1} = \tilde{u}_i^{n+1} - \frac{\Delta t}{\rho} \frac{\partial \Phi^{n+1}}{\partial x_i} \tag{11}$$

The LES solver

The LES solver used in our study is detailed in [15]. It is based on the mixed dynamic Smagorinsky sub-grid model. This dynamic model has shown to give satisfactory results for wall bounded flows, including the pipe flow [19]. Mass and momentum equations result from a spatial filtering of the Navier-Stokes equations (1-2). The JADIM code being based on a finite volume discretization, the natural filtering operator $\overline{G}$ is the box-filter, $\overline{G} = 1$ in the considered cell and $\overline{G} = 0$ otherwise. We use a uniform grid spacing Δ yielding the filter length to be $\overline{\Delta} = \Delta$. Applying $\overline{G}$, the velocity and pressure fields are decomposed as $u_i = \overline{u}_i + u_i'$ and $p = \overline{p} + p'$ where $\overline{u}_i$ (resp. u_i') and $\overline{p}$ (resp. p') are the resolved (resp. unresolved) contributions. The governing equations in the LES approach are then:

$$\frac{\partial \overline{u}_i}{\partial x_i} = 0 \tag{12}$$

$$\frac{\partial \overline{u}_i}{\partial t} + \frac{\partial \overline{u}_i \overline{u}_j}{\partial x_i} = -\frac{1}{\rho} \frac{\partial \overline{p}_i}{\partial x_i} + \nu \frac{\partial^2 \overline{u}_i}{\partial x_i \partial x_j} - \frac{\partial \tau_{ij}^{SGS}}{\partial x_j} + \overline{f}_{IBM,i} \tag{13}$$

where $\overline{f}_{IBM,i}$ is the filtered body force representing the solid/fluid interaction and $\tau_{ij}^{SGS} = \overline{u_i u_j} - \overline{u}_i \overline{u}_j$ is the sub-grid stress tensor (SGS) expressed as the sum of these three terms: L_{ij}, C_{ij} and R_{ij} such as:

$$L_{ij} = \overline{\overline{u}_i \overline{u}_j} - \overline{\overline{u}}_i \overline{\overline{u}}_j \tag{14}$$

$$C_{ij} = \overline{\overline{u}_i u'_j} + \overline{\overline{u}_j u'_i} - \overline{\overline{u}}_i \overline{u'}_j - \overline{\overline{u}}_j \overline{u'}_i \tag{15}$$

$$R_{ij} = \overline{u'_i u'_j} - \overline{u'}_i \overline{u'}_j \tag{16}$$

The Leonard term L_{ij} is calculted explicitly.

$$\tau_{ij}^{SGS} - \frac{1}{3}\tau_{kk}^{SGS}\delta_{ij} = -2\nu_T \overline{S}_{ij} + L_{ij} - \frac{1}{3}L_{kk}\delta_{ij} \tag{17}$$

where $\overline{S}_{ij}$ is the strain rate tensor calculated from the resolved velocity field and the turbulent viscosity ν_T is given by:

$$\nu_T = C\overline{\Delta}^2 (2\overline{S}_{ij}\overline{S}_{ij})^{\frac{1}{2}} \tag{18}$$

with $\overline{\Delta}$ is the filter length. C is a local parameter calculated at each time step. By re-filtering eq (13) using $\widetilde{\Delta}$, we define: $T_{ij} = \widetilde{\overline{u_i u_j}} - \widetilde{\overline{u}}_i \widetilde{\overline{u}}_j$. Similary as τ_{ij}^{SGS}, T_{ij} is also expressed in function of C as:

$$T_{ij} - \frac{1}{3}T_{kk}\delta_{ij} = -2C\widetilde{\overline{\Delta}}^2 |\widetilde{\overline{S}}|\widetilde{\overline{S}}_{ij} + L_{ij}^T - \frac{1}{3}L_{kk}^T\delta_{ij} \tag{19}$$

with $L_{ij}^T = \widetilde{\overline{\overline{u}_i \overline{u}_j}} - \widetilde{\overline{\overline{u}}}_i \widetilde{\overline{\overline{u}}}_j$. Both T_{ij} and $\widetilde{\tau^{SGS}}_{ij}$ cannot be calculated explicitly however the difference $l_{ij} = T_{ij} - \widetilde{\tau^{SGS}}_{ij} = \widetilde{\overline{u}_i \overline{u}_j} - \widetilde{\overline{\overline{u}}}_i \widetilde{\overline{\overline{u}}}_j$ can be and allows to find the local coefficient C:

$$l_{ij} - \frac{1}{3}l_{kk}\delta_{ij} = -2C(\widetilde{\overline{\Delta}}^2 |\widetilde{\overline{S}}|\widetilde{\overline{S}}_{ij} - \widetilde{\overline{\Delta}^2 |\overline{S}|\overline{S}_{ij}}) - \widetilde{\overline{\overline{u}}}_i \widetilde{\overline{\overline{u}}}_j + \widetilde{\overline{\overline{u}}_i \overline{\overline{u}}_j} + \frac{1}{3}(\widetilde{\overline{\overline{u}}}_k \widetilde{\overline{\overline{u}}}_k - \widetilde{\overline{\overline{u}}_k \overline{\overline{u}}_k})\delta_{ij} \tag{20}$$

C is then:

$$C = -\frac{(l_{ij} - h_{ij})M_{ij}}{2M_{ij}M_{ij}} \tag{21}$$

with $M_{ij} = \widetilde{\overline{\Delta}}^2 |\widetilde{\overline{S}}|\widetilde{\overline{S}}_{ij} - \widetilde{\overline{\Delta}^2 |\overline{S}|\overline{S}_{ij}}$ and $h_{ij} = \widetilde{\overline{\overline{u}_i \overline{u}_j}} - \widetilde{\overline{\overline{u}}}_i \widetilde{\overline{\overline{u}}}_j$

Coupling IBM and LES solvers

The IBM-LES coupling consists in applying the numerical procedure described above for the IBM method to the governing equations considered for LES simulations. The IBM coupling term is then expressed using the filtered velocity field:

$$\overline{f}_{IBM,i}^k = \alpha_{IBM} \frac{v_{s,i}^{k-1} - \overline{u}_i^k}{\Delta t} \tag{22}$$

The JADIM LES solver has been implemented and validated in previous studies: channel flows [15] and pipe flows [19]. However, the LES solver has been applied with a refined mesh having four to five cells across the viscous sub-layer in order to switch to DNS close to the wall. The aim of the current work is to couple this IBM-LES method with an appropriate wall modeling to make possible high-Reynolds simulations on a coarse mesh.

2.2 The numerical set-up

We consider a pipe of diameter $D = 2R$ and axis Ox inside a box of size $L_x \times L_y \times L_z$ along the e_x, e_y and e_z directions, respectively (Fig. 1). The domain is described using a regular mesh with cells of size Δ along the three directions. The definition of the solid volume fraction requires an explicit definition of the geometry (as for any boundary in CFD). If the geometry is simple enough to be described analytically, as it is the case in the present paper, we have access to the analytical expression for the solid volume fraction. For complex geometries, for which no analytic description can be used, we can use instead files describing the position of the walls coming from CAD, but the definition of $\alpha_{IBM}(\mathbf{x})$ is not an issue. Specifically, we have proposed in [20, 21] a method which consists of using the function 'distance' of the CFD free-software BASILISK which builds a distance field from an STL file and converts it to determine the volume

fraction α_{IBM}. α_{IBM} is saved as a function of the cells coordinates in a file and imported as an input for our CFD JADIM code. For the pipe geometry considered here, the solid volume fraction α_{IBM} is given by [18]:

$$\alpha_{IBM}(\mathbf{x}) = \frac{1}{2}\left[1 - \tanh\left(\frac{r-R}{\sqrt{2}\lambda\eta\Delta}\right)\right] \tag{23}$$

where r is the distance to the pipe center, $\lambda = \mid n_x \mid + \mid n_y \mid + \mid n_z \mid$ is calculated using the coordinates of $\mathbf{n}$ the normal outward unit vector at the cylinder surface and $\eta = 0.065(1-\lambda^2) + 0.39$ is a parameter controlling the thickness of the transition region between the solid $\alpha_{IBM} = 1$ and the fluid $\alpha_{IBM} = 0$. This relation for λ suppresses parasitic fluctuations of the forces applied to the object when the latter crosses a numerical cell [17]. With expression (23), the cylinder wall corresponds to the value $\alpha_{IBM} = 0.5$ as shown in Fig. 1 and the transition from the fluid to the solid corresponding to $0 < \alpha_{IBM} < 1$ is spread over three cells. In the following, this region ($0 < \alpha_{IBM} < 1$) will be called "IBM wall thickness".

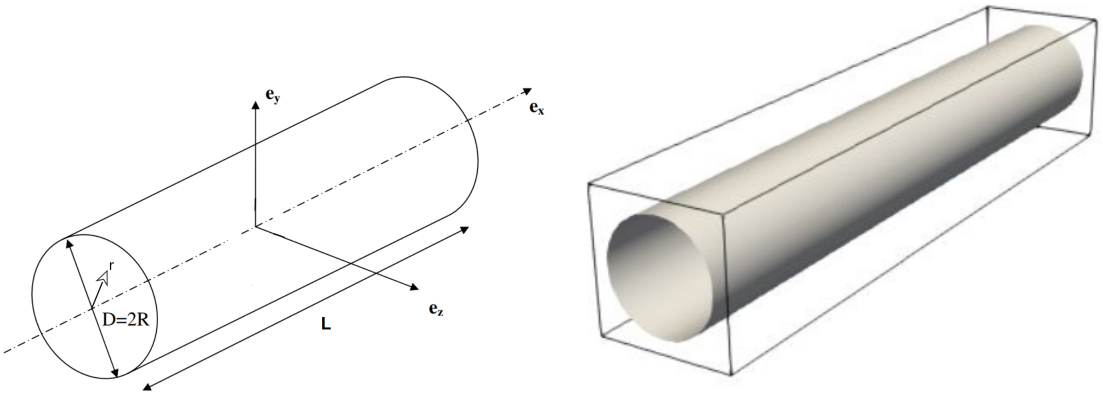

Figure 1: Sketch of the geometry (left). Numerical domain and wall pipe shown using the iso-contour $\alpha_{IBM} = 0.5$ (right).

Four different uniform regular Cartesian meshes $m1, m2$, $m3$ and $m4$ are considered corresponding to the number of cells per pipe radius $R/\Delta = 8$, $R/\Delta = 16$, $R/\Delta = 32$ and and $R/\Delta = 64$, respectively. Figure 2 represents the mesh on a cross section of the pipe. As shown, the solid wall thickness decreases when the mesh is refined.

The flow is driven by a fixed pressure drop dp/dx along the x-direction. Periodic boundary conditions at the inlet and outlet of the pipe are imposed. The flow is characterized by the Reynolds number $Re = D < U > /\nu$ with $< U >$ the bulk velocity. The domain length L_x is fixed to $5D$ allowing developing the turbulence and $L_y = L_z = 1.2D$.

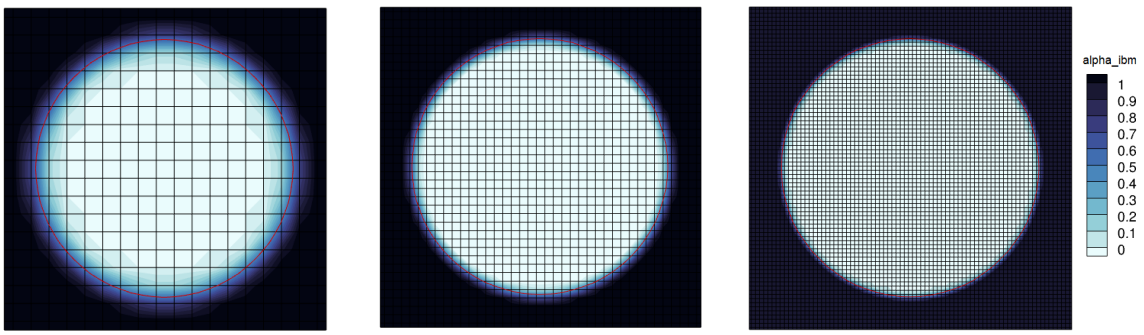

Figure 2: Pipe cross-section for the three meshes $m1$ ($R/\Delta = 8$), $m2$ ($R/\Delta = 16$), and $m3$ ($R/\Delta = 32$) from left to right. The corresponding IBM function field is shown from $\alpha_{IBM} = 0$ (white) to $\alpha_{IBM} = 1$ (black).

The temporal accuracy of the Navier-Stokes solver has been discussed in a series of papers. In particular, we refer to [15] where the LES approach has been first proposed. In this paper, the temporal accuracy of the code, a crucial requirement when dealing with turbulent flows, is shown with a test devoted to the evolution of two-dimensional small-amplitude disturbances in a plane channel flow, following a test proposed by [22] and [23]. Concerning the time convergence of the IBM forcing, we refer to Bigot et al. [17] where the case of an oscillating sphere in a fluid initially at rest is considered. Almost first order convergence in time was observed. We have further verified for both the laminar and the turbulent pipe flow that the variation of the time step has no effects on the reported results. For example, we have solved the Poiseuille flow with the wall model on mesh $m2$ considering three different time steps $0.2t_{CFL}$, $0.4t_{CFL}$ and $1t_{CFL}$, t_{CFL} being the Courant Friedrichs Lewy characteristic time equal to Δ/u with Δ is the mesh size and $u = \nu Re/D$ is the bulk velocity. Regardless of the time step, we have observed that the relative errors for the velocity and the shear stress are the same relative error proving that the simulation converges to the same solution independently of the time step. We have not reported these tests to avoid lengthening the paper.
The spatial convergence is shown in the next section for the Poiseuille flow considering both the velocity field and the shear stress. However, for the simulation of the turbulent pipe flow with the LES-IBM simulation, the approach is different because we aim at providing a model to make possible simulation on a coarse grid, with parameter dependent on the grid size. Thus, the parameters of the model are indeed mesh-size dependent. It is actually a required feature, as the model should vanish in case the resolution is fine enough.

3 Poiseuille flow

We first consider the case of laminar Poiseuille flow to evaluate the ability of IBM to predict the flow in a circular pipe. The selected Reynolds number is Re=460 and the exact solution for the velocity U and shear stress τ are:

$$U(r) = -\frac{1}{4\mu}\frac{dp}{dx}\left(R^2 - r^2\right) , \quad \tau(r) = -\frac{1}{2}\frac{dp}{dx}r \tag{24}$$

At first, numerical simulations are carried out using the standard IBM expression (7) to prescribe the presence of the wall. Figure 3 compares the velocity profile $U(r)$ and the shear stress $\tau(r)$ to the exact solution for the three meshes $m1$, $m2$ and $m3$. $U(r)$ and $\tau(r)$ are respectively made dimensionless by the maximum central velocity $U_{max} = -\frac{1}{4\mu}\, dp/dx R^2$ and the wall shear stress $\tau_{wall} = -\frac{1}{2}\, dp/dx R$ given by the exact solution (24). We consider the error relative to the analytical solution. We evaluate both the error for the velocity at the IB wall ($r = R$) as:

$$\epsilon_{U(R)} = \frac{|U(R)^{analytical} - U(R)^{simulation}|}{U(0)^{analytical}} , \tag{25}$$

and the relative error of the shear stress at two positions, at the IB wall $r = R$ and in the bulk of the fluid $r = R/2$, as

$$\epsilon_{\tau(r)} = \frac{|\tau(r)^{analytical} - \tau(r)^{simulation}|}{\tau(r)^{analytical}} . \tag{26}$$

The evolution of the errors with the grid size is presented in Fig. 4. We observe that the rate of convergence of the velocity and the shear stress at the IB wall using the standard IBM expression (7) with no model is, as expected, lower than second order.

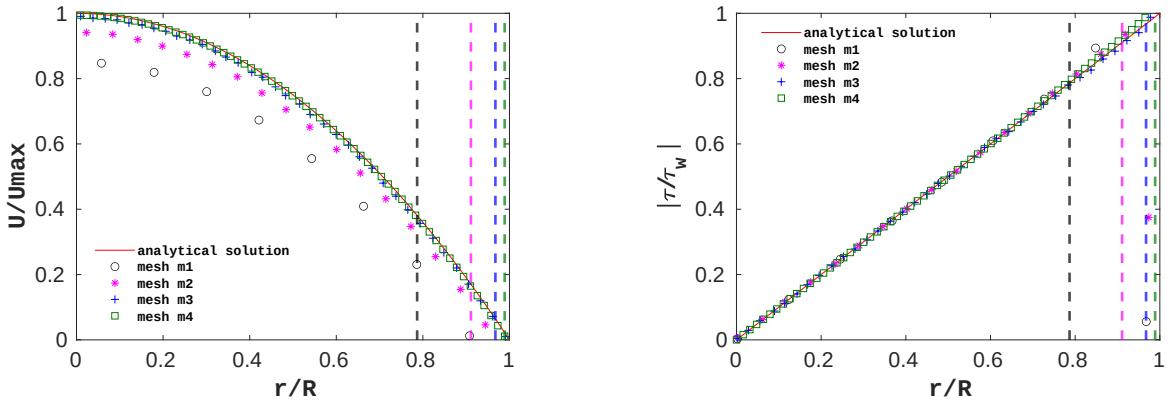

Figure 3: Dimensionless radial profiles of the velocity (left) and the shear stress (right) for the four meshes with the standard IBM approach, compared to the exact solution given by eq. (24). The vertical dashed lines mark out the limit between the fluid and the IBM region ($\alpha_{IBM} > 0$) for each mesh.

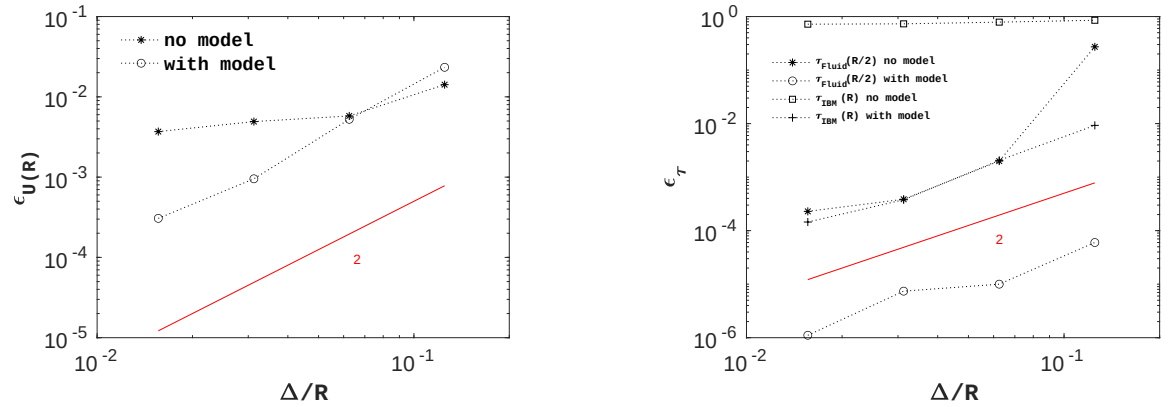

Figure 4: Grid convergence of the relative error on $U(R)$ the velocity at the IB wall (left), and of the shear stresses $\tau_{IBM}(R)$ and $\tau_{Fluid}(R/2)$ at the IB wall ($r = R$) and in the fluid at $r = R/2$, respectively.

The significant loss of accuracy close to the wall is the direct consequence of the IBM solid-fluid interaction description used for the simulation. In the standard method first applied here, a zero velocity is considered across the entire IBM wall thickness zone i.e. for $0 < \alpha_{IBM} \leq 1$. We clearly observe in Fig. 3 that the resulting viscous shear stress departs from the linear evolution in this region and this impacts the shear stress in the fluid close to the wall.

The control of the velocity profile cannot be made with the IBM function given by equation (23) since it mainly controls the width of the IBM wall thickness. The proposed method consists in directly imposing the correct velocity evolution inside the IBM wall thickness. In the case of the Poiseuille flow the exact solution is given by equation (24) therefore, the corresponding velocity profile for the solid wall velocity v_s for the solid-fluid interaction description is then:

$$v_{s,x}(r) = -\frac{1}{4\mu}\frac{dp}{dx}(R^2 - r^2)\,, \quad v_{s,y} = v_{s,z} = 0 \tag{27}$$

By the definition of f_{IBM}, this forcing is effective for $\alpha_{IBM} > 0$. The velocity profile in the IBM wall thickness cancels at the exact wall position $r = R$ corresponding to $\alpha_{IBM} = 0.5$. Note that the velocity for $r > R$ is then negative in order to respect the correct value of the velocity gradient, and thus the wall shear stress at $r = R$. Figure 5 presents the velocity and shear stress obtained with the new IBM condition (27). All the profiles are now very close to the analytical solution regardless of the mesh size.

The corresponding errors on both the velocity and the viscous shear stress are reported in Fig. 4 as a function of the grid size. We also observe that with the proposed modification of the IBM forcing, the magnitude of the error has been significantly reduced and convergence close to second order is observed for both velocity and shear stress. Note that correcting the velocity in the region $0 < \alpha_{IBM} \leq 0.5$ only, does not permit to recover the correct shear stress at the wall $r = R$.

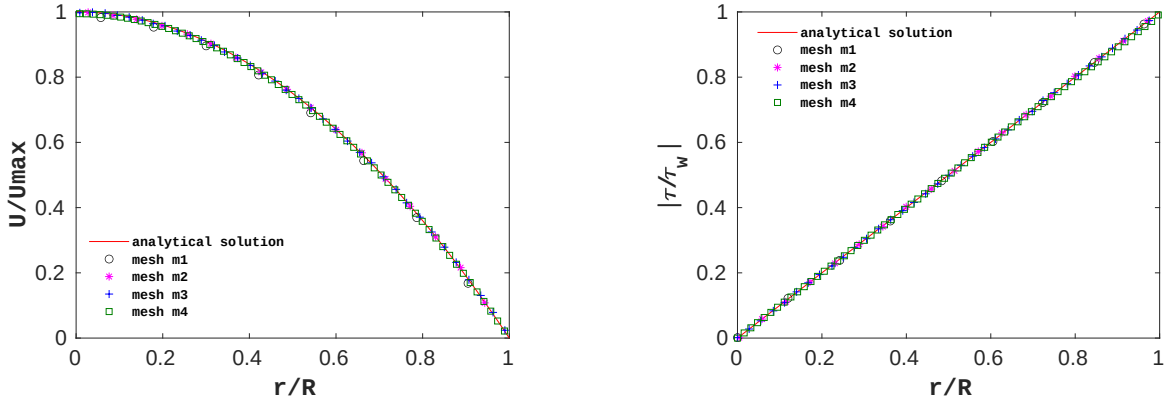

Figure 5: Dimensionless profiles of the velocity and the shear stress when using the IBM wall model (27)

From the DNS simulation of a Poiseuille pipe flow, we have demonstrated that the IBM method using the standard solid-fluid interaction is grid convergent. However the error with the exact solution can be significantly reduced with an appropriate condition applied inside the region of IBM wall thickness. The objective of the next section is to consider turbulent pipe flow simulations thanks to our IBM-LES solver.

4 Turbulent pipe flow

In this section, we simulate turbulent pipe flows using the IBM-LES method and using the same numerical domain. The flow is again driven by a constant pressure drop. We note $< U >$ the bulk velocity, $\tau^* = R|dp/dx|/2$ the mean wall shear stress, $u^* = \sqrt{\tau^*/\rho}$ the mean friction velocity, $\ell^* = u^*/\nu$ the wall unit length, $Re^* = Ru^*/\nu$ the friction Reynolds number and $Re =< U > D/\nu$ the pipe Reynolds number. Three high Reynolds numbers are considered: $Re = 50,000$, $Re = 100,000$ and $Re = 500,000$.

Discussion on the results will be first conducted for $Re = 100,000$ because several reference results are available at this specific Reynolds number for the mean axial velocity profile U and the root mean square (RMS) velocities u_x, u_r, u_θ along the x, r and θ directions, respectively. The corresponding references, values of Re and Re^* are reported in table 1.

Method	References	Re	Re^*	Available radial distributions	symbol in graphs
LES/RANS	[14]	100,000	2350	$U(r)$	$\times$
Experiments	[11]	98,000	2315	$U(r)$	$\wedge$
DNS	[13]	83,000	2000	$U(r)$, $u_x(r)$, $u_r(r)$, $u_\theta(r)$	$\diamond$
Experiments	[12]	81,000	1960	$U(r)$, $u_x(r)$	$+$

Table 1: References used for comparison and corresponding symbols used in the figures.

The simulations are performed using the three meshes $m1$, $m2$ and $m3$. The ratio Δ/ℓ^* is reported in Table 2 for the three considered Reynolds numbers. With regard to high turbulent pipe flows, these meshes are coarse and none of them is adapted for an accurate resolution of the viscous sub-layer, justifying the need of an appropriate wall modeling. This is clearly shown in Fig. 6 where the simulations performed

using mesh $m2$ are compared to the data referenced in Table 2 for $Re = 100,000$. As reported, all the data from literature are collapsing on a similar evolution for the mean velocity U. The LES-IBM simulation using the standard IBM solid-fluid interaction presented by circles is significantly underestimating the mean velocity indicating that the wall friction is not correctly predicted. This response of the model is very similar to what we observed for a laminar flow. Considering the velocity fluctuations, thanks to the LES solver, their order of magnitude is correctly captured inside the pipe but not close to the wall. The objective is now to propose a modified IBM solid-fluid interaction in order to improve the results and in particular to recover the correct magnitude for the mean velocity. Two approaches will be proposed in the following; the first one is based on the mean velocity profile while the second makes use of a stochastic model for the velocity profile imposed across the IBM wall thickness.

R/Δ - Re	50,000	100,000	500,000
8 ($m1$)	160	292	1260
16 ($m2$)	80	146	630
32 ($m3$)	40	73	315

Table 2: Value of ratio Δ/ℓ^* for the meshes and Reynolds numbers considered

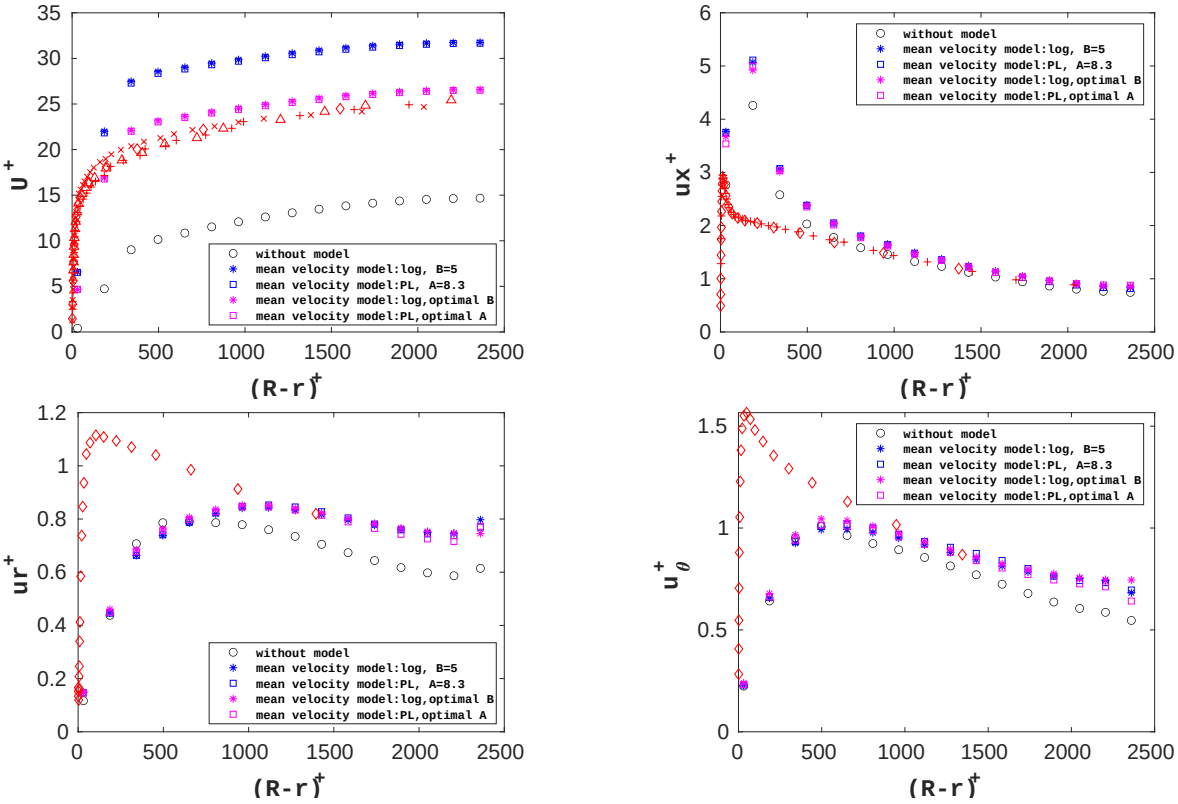

Figure 6: Profiles of the mean velocity and RMS velocity for simulations at Re=100,000 for different IBM approaches. Top left: mean velocity; top right: axial velocity RMS; bottom left: radial velocity RMS; bottom right: azimuthal velocity RMS. Simulation using the standard IBM solid-fluid interaction without a wall model (o), with the power laws mean velocity model (□) and with the logarithmic mean velocity model ($*$). For the mean velocity models, results with the classical coefficients (in blue): $k = 0.41 - B = 5$ and $A = 8.3 - C = 1/7$ for the "log-law" and "power law" laws, respectively. Results with the adjusted coefficients (in purple): $k = 0.41 - B = 0$ and $A = 5.3 - C = 1/7$ for the "log-law" and "power law" laws, respectively. Red symbols stand for the reference studies: $\times$[14], $\wedge$, [11], $\diamond$[13], $+$[12] (see Table 1)

4.1 IBM mean velocity model

In the case of turbulent pipe flow, no exact solution for the velocity profile is available to control the unsteady and local velocity field inside the IBM wall thickness as done in the previous section for the laminar Poiseuille flow. However the mean velocity profile close to a turbulent wall in a pipe has been characterized for a large range of Reynolds numbers. In particular the mean velocity can be described by the classical log-law evolution or can be fitted by a power law. Both laws have been considered at high Reynolds number regimes in experimental and numerical studies. See for example [24] where both laws compare well with LES simulations over a large range of Reynolds numbers varying from 10^4 to 10^{11}.

In this section, both the "log-law" and "power law" modeling are selected to control the velocity description inside the IBM wall thickness. Since the model has to be implemented across the entire IBM thickness, a velocity condition has to be imposed for $0.5 < \alpha_{IBM} < 1$, i.e. for negative values of the wall unit distance $r^+ = (R - r)/\ell^*$. In order to respect the condition $v_s(r^+ = 0) = 0$ and the continuity of the velocity for discretization purpose in the viscous shear calculation, the velocity field is extended for $r^+ < 0$ (i.e. $r > R$). Under these considerations, the "log law" modeling consists in imposing in the IBM fluid-coupling term f_{IBM} defined by (3) the velocity field v_s following:

$$v_{s,x} = \begin{cases} r^+ \ < u^* > & \text{if } \mid r^+ \mid \leq 11 \\ \text{sign}(r^+) \, (\frac{1}{k} log(\mid r^+ \mid) + B) \ < u^* > & \text{if } \mid r^+ \mid > 11 \end{cases}, \quad v_{s,r} = v_{s,\theta} = 0 \tag{28}$$

with $k = 0.41$ and $B = 5$ [25], while the "power law" modeling considers

$$v_{s,x} = \begin{cases} r^+ \ < u^* > & \text{if } \mid r^+ \mid \leq 11 \\ \text{sign}(r^+) \, A \mid r^+ \mid^C < u^* > & \text{if } \mid r^+ \mid > 11 \end{cases}, \quad v_{s,r} = v_{s,\theta} = 0 \tag{29}$$

with $A = 8.3$ and $C = 1/7$ [26].

To analyze the effect of such control of the velocity in the IBM wall thickness, numerical simulations are first performed for $Re = 100,000$ using mesh $m2$. Figure 6 illustrates the mean and RMS profiles normalized by u^* as a function of the radial position normalized by the wall unit length ℓ^*. The two models ("log law" and "power law") provide very similar results for both the mean and the RMS velocities. The mean velocity profile is now overestimated in comparison with the previous data from literature. The impact on the RMS velocity differs depending on each component. The velocity fluctuation in the streamwise direction increases close to the wall and is improved far from it in the two other directions. The peak of the streamwise fluctuations generally located around $15\ell^*$, considered as a feature of turbulent pipe flow, cannot be detected with such a mesh resolution (see Table 2). However we see a peak in our profiles which is shifted away from the near wall with a higher intensity. Similar behavior of the peak location is reported by Ma [9] using a dynamic wall model for LES/IBM simulations. Besides, the simulations on other meshes reveal that the peak gets closer to the wall as we refine the mesh. The results obtained with the model follow the expectations but still need to be adapted and one possible solution to do so is through the modification of the wall law coefficients. An adjustment of the coefficients B for the log law and A for the power law is performed aiming at minimizing the error on the bulk velocity. Figure 7 depicts the relative error on the bulk velocity as a function of the wall law coefficients for the mesh $m2$. The reported error E_U is calculated as:

$$E_U = \frac{< U >^{expected} - < U >^{simulation}}{< U >^{expected}} \tag{30}$$

where $< U >^{expected}$ is the expected value of the bulk velocity based on the pressure drop imposed to the pipe flow and $< U >^{simulation}$ is the one given by the simulation. Positive values represent the case of an underestimate of the bulk velocity as observed with no wall model giving $E_U = 55\%$. As shown in Fig. 6, using the two considered wall models induces an overcompensation of the mean velocity with a relative error $E_U = -20\%$. Thus, by adjusting the values of the model coefficients, an optimal value of $B \approx 0$ and $A \approx 5.8$ for the log and power models, respectively, can be found with a relative error less than 1%.

Our results show that changing the value of B from $B = 5$ to $B = 0$ improves the results. Let us note that in fully developed turbulent flows the von Karman constant (the multiplicative constant in front of the log) is observed to be nearly universal, whereas the additive constant B is found to vary for different flows or types of boundary (e.g. roughness of the wall). This is consistent with the control of the flow inside the IBM walls, which legitimates the choice for only changing the B constant.

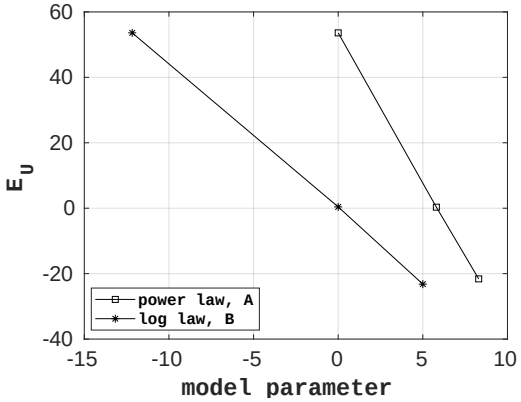

Figure 7: Relative error E_U on the mean flow rate as a function of the wall law coefficients B and A for the log and power models, respectively.

The flow statistics when using these coefficients are reported in Fig. 6 and discussed in section 4.3. As shown, with the adapted wall law coefficient, it is possible to obtain accurate mean velocity profiles. However, in terms of velocity fluctuations, the model does not improve remarkably the RMS in comparison with the basic model. The reason is that the model is based on a constant and uniform friction velocity without introducing any source of fluctuations. And this can justify two main features of this model:
- the need of adjusting the wall law coefficient. For instance, the simulation using the classical law yields higher bulk velocity because it does not have enough fluctuations, the latter contributing to the mean shear and can restore the correct mean velocity profile. In short, it is not just about controlling the bulk velocity but also acting on the fluctuations.
- the RMS velocities remain unchanged for different values of the wall law coefficients which means that tuning the wall law coefficient may not be the relevant approach if we are interested in reproducing the fluctuations as well, keeping in mind that a precise agreement remains challenging if considering coarse meshes.
Therefore, we can conclude that the model based on the mean friction velocity overestimates the bulk velocity and needs to be corrected by an appropriate modeling for the fluctuations. Indeed, if we manage to increase the fluctuations, the mean velocity will decrease and it will be automatically corrected with no need of tuning the wall law coefficients. This is the objective of the stochastic wall model proposed in the next section.

4.2 Stochastic velocity model

The previous model based on the mean friction velocity may be improved by taking into account some fluctuations in the velocity imposed across the IBM wall thickness. Indeed, the wall region is known to present significant fluctuations with characteristic spatial and temporal correlations resulting from the regeneration cycle of turbulent structures as well as from the interaction with the outer flow [27, 28]. It has been pointed out [29] that the complex flow structure is strongly correlated to the wall shear stress which thus presents large-scale fluctuations [30, 29, 31].

To mimic the effect of the unresolved turbulent wall structures, we propose to use a stochastic field which reproduces the fluctuations of the wall shear stress, for the definition of the solid velocity field v_s

used for IBM fluid-solid coupling term f_{IBM} (3). Reflecting the view of the momentum cascade taking place in the logarithmic layer as a self-similar hierarchy of wall-attached eddies [32, 33], we express the local IBM velocity from the law of the wall, but substituting the average friction velocity by a random friction velocity:

$$v_{s,x}(r,\theta,x,t) = \begin{cases} r^+ \, u^*(\theta,x,t) & \text{if } \mid r^+ \mid \leq 11 \\ \text{sign}(r^+) \, (\frac{1}{k} log(\mid r^+ \mid) + B) \, u^*(\theta,x,t) & \text{if } \mid r^+ \mid > 11 \end{cases}, \quad v_{s,r} = v_{s,\theta} = 0 \tag{31}$$

while keeping the original values of $k = 0.41$ and $B = 5.0$.
Note that the length scale l^* used to normalize r remains constant and is based on the average friction velocity. This model is supported by the self-similarity of large scales leading the velocity profile to scale with u^* as reported in [30, 31].

In order to reproduce the very large deviations of the wall shear stress [29], we assume that the stochastic field $u^*(\theta,x,t)$ presents a log-normal distribution [34, 35]. Then the variable $f = \ln(u^*/\langle u^* \rangle)$ has a normal distribution with average μ and variance σ^2. From the expression of the moments of log-normal variables $\langle (e^f)^q \rangle = e^{q\mu + q^2\sigma^2/2}$, we impose for its average $\mu = -\sigma^2/2$ to have $\langle e^f \rangle = 1$ and balance the global momentum budget. Considering that the variance of u^* is commensurate with the square of its mean, we introduce the ratio $\alpha_h = \langle u'^{*2} \rangle / \langle u^* \rangle^2$ which is related to σ as $\sigma^2 = \ln(1+\alpha_h)$. Indeed [36] showed that the standard deviation of u^* is between 15% and 40% of its mean value from experimental and DNS data and is probably Reynolds number dependent. We also want to impose the spatial correlation lengths in the streamwise and spanwise directions as well as the temporal correlation to account for both lifetime of the turbulent structures and their advection by the mean flow. These spatiotemporal correlations of the wall shear stress have been reported in [31, 30, 29]. It has been observed that the correlation lengths in the streamwise and spanwise directions are around 1000 and 100 wall units respectively, similarly to the near-wall flow structures [37, 38, 39, 40]. We expect the convection velocity of the wall friction to be scale-dependent [41, 30, 42]. Indeed, the large scales of the wall friction, which are related to events taking place in the logarithmic region have been reported to be convected at a velocity that is much faster than the average speed in the near-wall region [30, 43], while the smaller scales which are due to the near-wall cycle which append in the buffer layer are convected with the characteristic speed of the buffer layer [41, 42]. Overall, the convection velocity, in wall unit, is estimated to stand in the range $u^+_{adv} = 10 - 20$ [30, 42].

To model the wall friction field, we generate initially a field without spatial correlations (delta-correlated in space) but presenting a temporal correlation obtained by the resolution of a stochastic differential equation. Then, in a second step this field is convoluted with a spatial kernel to impose the adequate spatial correlation prescribed by the shape of the convolution kernel. The last step consists in taking the exponential of the field to obtain a log-normal field.

According to this procedure, we have:

$$f(t,\mathbf{x}) = \int G(\mathbf{x} - \mathbf{x'}) \chi(t,\mathbf{x'}) d\mathbf{x'} \tag{32}$$

where the stochastic process with delta-correlation in space is noted χ and G is a convolution kernel with $\mathbf{x}(x_x, x_\theta)$ and $\mathbf{x'}(x'_x, x'_\theta)$ position vectors. Note that the spatial autocorrelation of f is only set by G since χ is delta-correlated $\rho_f(\mathbf{x}) = G \star G$ where $\star$ denotes the convolution product.

To deem the advection, we decompose the convolution kernel into two parts: $G = G_s \star \delta(\mathbf{x} - \mathbf{u}_{adv} t)$, the second contribution representing the spatial translation due to the advection at a constant speed $\mathbf{u}_{adv}$. We propose to model the spatial contribution G_s as:

$$G_s(\mathbf{x}) = \beta \exp\left[-\left(\frac{x_x}{L_{cx}}\right)^2 - \left(\frac{x_\theta}{L_{c\theta}}\right)^2 \right] \tag{33}$$

and β is a pre-factor for normalization purpose. L_{cx} and $L_{c\theta}$ are the characteristic lengths in the streamwise and the spanwise directions respectively and are first set to $L_{cx} = 1000\ell^*$ and $L_{c\theta} = 100\ell^*$. In the current study, we take the advection velocity in the streamwise direction with a magnitude set to $u_{adv} = 20\langle u^* \rangle$.

We consider that the field χ is the solution of a stochastic differential Langevin equation defined and solved for each cell in the domain and at each time step:

$$d\chi = -\frac{\chi - \mu_\chi}{T_c} dt + \sqrt{\frac{2\sigma_\chi^2}{T_c}} dW \tag{34}$$

where dW is an increment of the Wiener process, a normal variable generated for each cell at each time step with $< dW >= 0$ and $< dW(t, \mathbf{x}) dW(s, \mathbf{x'}) >= \delta(t-s)\delta(\mathbf{x}\text{-}\mathbf{x'})$. In equation (34) the parameter μ_χ and σ_χ^2 are respectively the mean and the variance of χ, while T_c corresponds to the correlation time of χ. Here we have estimated the lifetime of the wall friction events as $T_c = L_{cx}/u_{adv}$. From (32) the moments of f and χ are related, therefore we impose for μ_χ and σ_χ^2:

$$\mu_\chi =< f > (\int G(r)dr)^{-1} = -\frac{1}{2}\ln(1+\alpha_h)(\int G(r)dr)^{-1} \tag{35}$$

$$\sigma_\chi^2 =< f'^2 > (\int G^2(r)dr)^{-1} = \ln(1+\alpha_h)(\int G^2(r)dr)^{-1} \tag{36}$$

Taking advantage of the periodicity in the x and θ directions, we compute the convolution product in the spectral space through the Fourier transform making the calculation much faster:

$$\mathcal{F}(f) = \mathcal{F}(G_s)\exp(i\mathbf{k}.\mathbf{u}_{adv}t)\mathcal{F}(\chi) \tag{37}$$

with $i^2 = -1$ and $\mathbf{k}$ the wave vector. The inverse Fourier transform allows us to obtain f and finally the friction velocity field writes as follows:

$$u^* =< u^* > exp(f) \tag{38}$$

We present in Fig. 8 a realization of the field obtained with this stochastic model (see also the movie in supplementary material). We observe that the model reproduces elongated structures moving with the prescribed velocity $\mathbf{u}_{adv}$ as expected.

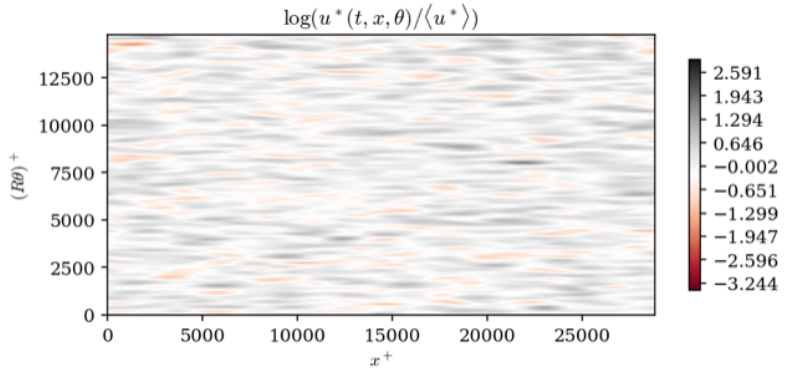

Figure 8: Realization of the stochastic process to predict the friction velocity field at the wall.

The main control parameter of the stochastic model is α_h which imposes the magnitude of the fluctuations. It is to note that α_h being the variance of $u^*/< u^* >$, setting $\alpha_h = 0$ restores the model with constant friction velocity presented in the previous section. To study the effect of α_h on the flow statistics,

we carried out simulations of the pipe flow with an expected value of $Re = 100,000$ with the mesh $m2$ with $\alpha_h = 1$, $\alpha_h = 0.3$ and $\alpha_h = 0.07$. Figure 9 shows the mean velocity and the velocity fluctuations as a function of the distance from the wall normalized by $\langle u^* \rangle$ and ℓ^*. As expected, the stochastic IBM velocity is effectively acting on the velocity fluctuations. Increasing α_h leads to a significant increase of the RMS of the three components of the velocity all across the pipe section. In particular, we notice the presence of a near-wall peak for both spanwise and wall normal components which were not present in the simulation without model. For $\alpha_h = 0.07$ we observe that the profile of the RMS of the various velocity components are in good agreement with the experimental data, expected for the first two points away from the wall.

Adding fluctuations in IBM region enhances the shear stress and consequently leads to a flattened mean velocity profile and causes a reduction of the bulk velocity. For the largest values of α_h it is clear that the level of fluctuations is too high and gives an under-prediction of the bulk velocity, but for $\alpha_h = 0.07$, the mean velocity appears to match the experimental data fairly well. This is confirmed in Fig. 10 that presents the relative error on the mass flow rate E_U defined by relation (30) as a function of α_h. For $\alpha_h = 0$ one recovers an overestimate of the flow rate with $E_U = -22\%$, as already obtained with the mean velocity model (28) (see Fig. 7), while for $\alpha_h = 0.07$, which is consistent with the value reported in [36], the relative error is less than 1%.

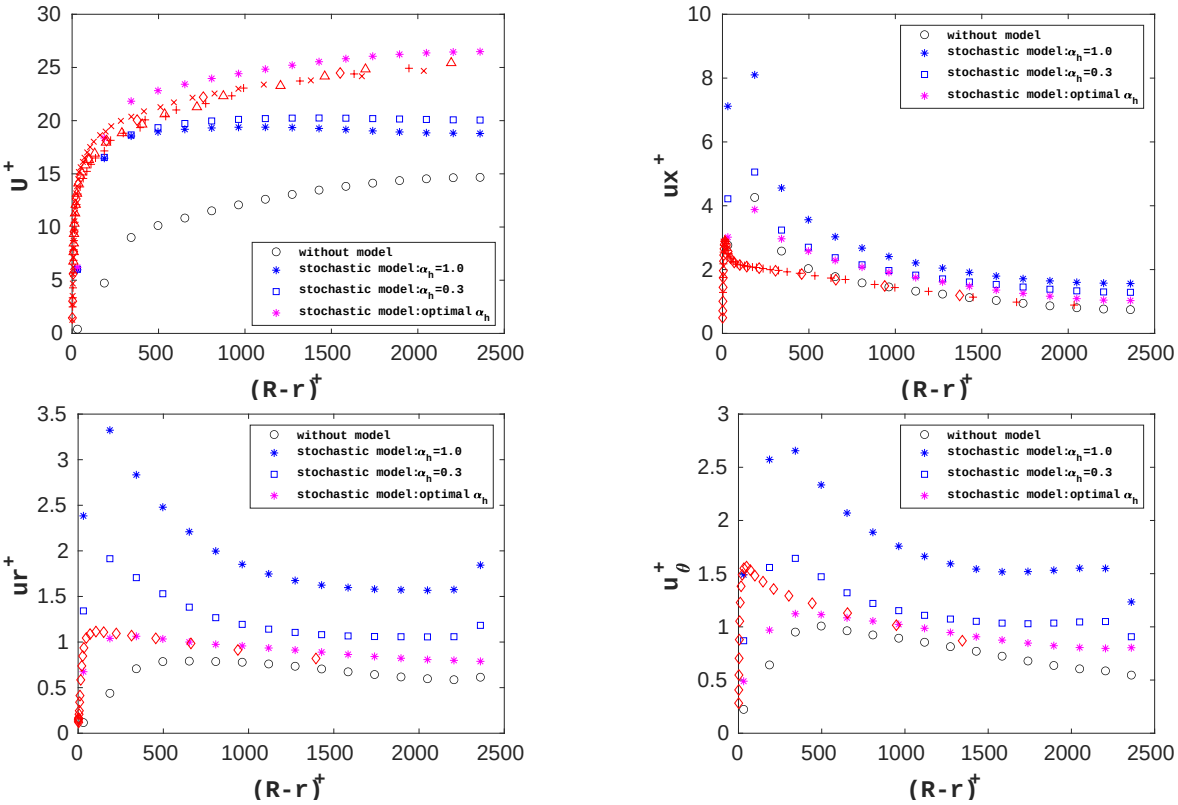

Figure 9: Comparison of the mean and RMS velocity profiles for $Re = 100,000$ obtained from the standard IBM without model (o) and with the stochastic wall model for 3 values of the α_h parameter: $\alpha_h = 1$ ($*$), $\alpha_h = 0.3$ ($\square$) and the optimal value $\alpha_h = 0.07$ ($*$). Red symbols stand for the reference studies: $\times$[14], $\wedge$, [11], $\diamond$[13], $+$[12] (see Table 1). Top left: mean velocity; top right: axial velocity RMS; bottom left: radial velocity RMS; bottom right: azimuthal velocity RMS.

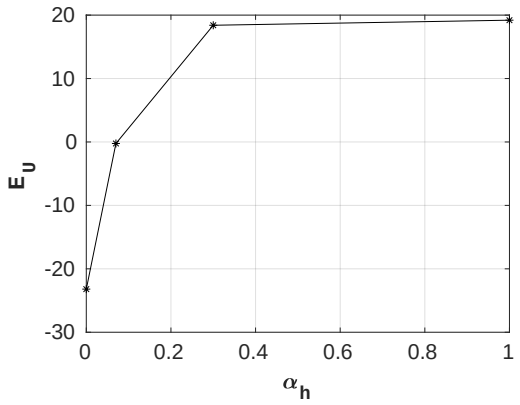

Figure 10: Relative error E_U on the mean flow rate, as defined in (30), for the IBM with stochastic wall model for $Re = 100,000$ as a function of the model parameter α_h.

4.3 Discussion

4.3.1 Model comparison

We now compare the different modeling approaches proposed in this work. The results are first presented in Fig. 11 for the mean and RMS velocity in order to make a direct comparison between the basic IBM wall model, the mean velocity model based on the log law and the stochastic model. Flow statistics are reported for the value of $B = 0$ for the "log law" model (28) and $\alpha_h = 0.07$ for the " stochastic" model (31) that reproduces for each model the correct bulk velocity for simulations on mesh $m2$. These models provide the same mean velocity profile and in good agreement with previous data. The log law relation (28) and the power law relation (29) are also plotted for comparison in blue and red lines, respectively. As observed, the fluctuations can be adjusted thanks to the use of a stochastic approach. More specifically, the intensity of the peaks in the near-wall region is improved: the peak is reduced in the streamwise direction while its magnitude is increased in the radial and azimuthal directions.

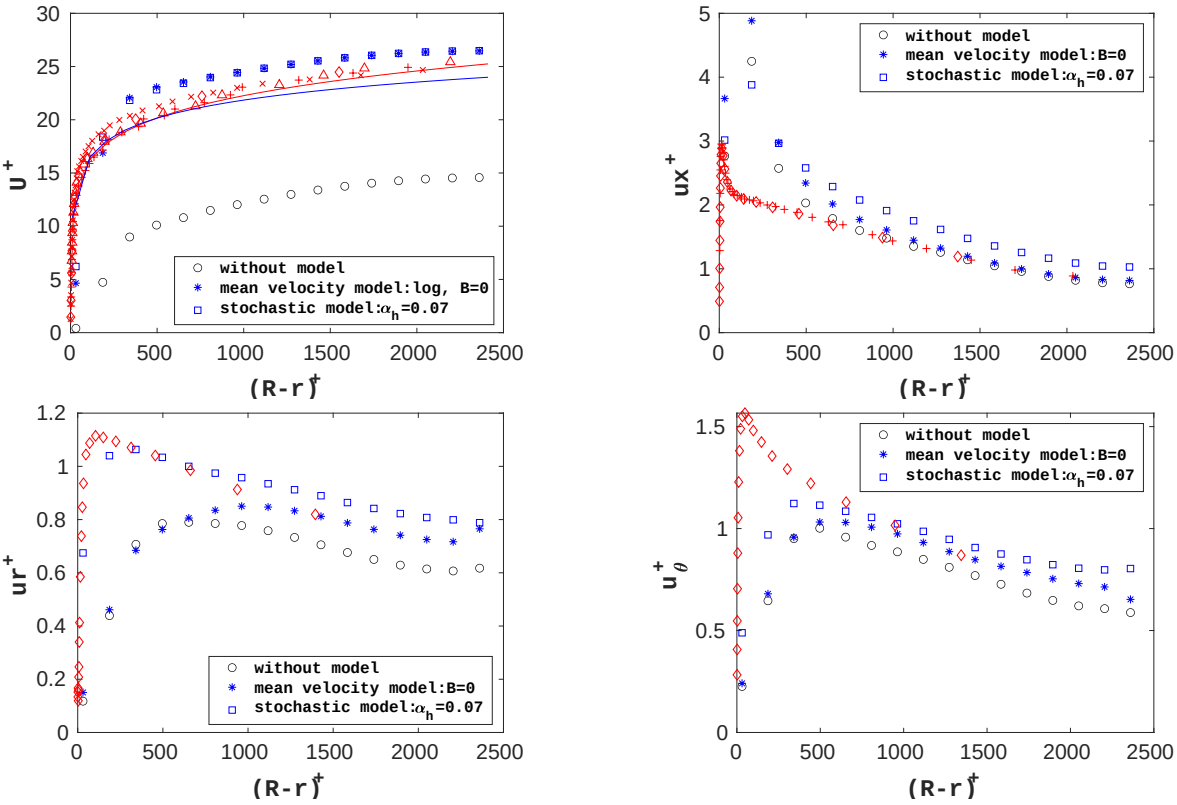

Figure 11: Comparison of the mean and RMS velocity profiles for $Re = 100,000$ obtained from the standard IBM without model (o) and with the mean velocity models ($*$) and the stochastic model ($\square$). Top left: mean velocity; top right: axial velocity RMS; bottom left: radial velocity RMS; bottom right: azimuthal velocity RMS. Red symbols stand for the reference studies: $\times$[14], $\wedge$, [11], $\diamond$[13], $+$[12] (see Table 1). Blue line: relation (28) for the "log law". Red line: relation (29) "power law".

We present in Fig. 12 the same plot as shown in Fig. 11 but with semi-logarithmic scales. Clearly, the semi-logarithmic plot outlines that both the mean velocity profile and the friction are improved with the use of a wall model. Especially we see that the logarithmic law of the wall can be reproduced with both the mean model and the stochastic model. Please note that because of our very coarse resolution there is no grid point in the near-wall region, which is the reason why a wall model is required. In Fig. 12, the vertical dashed line highlights the limit between the IBM region, $\alpha_{IBM} > 0$, and the plain fluid region, $\alpha_{IBM} = 0$. We can notice that the points within the IBM region present a gap with the reference, whereas the points lying outside the IBM region present a much better agreement. Overall, considering both Fig. 11 and 12 , the stochastic approach provides a better prediction of the fluctuating flow structures along the three spatial directions.

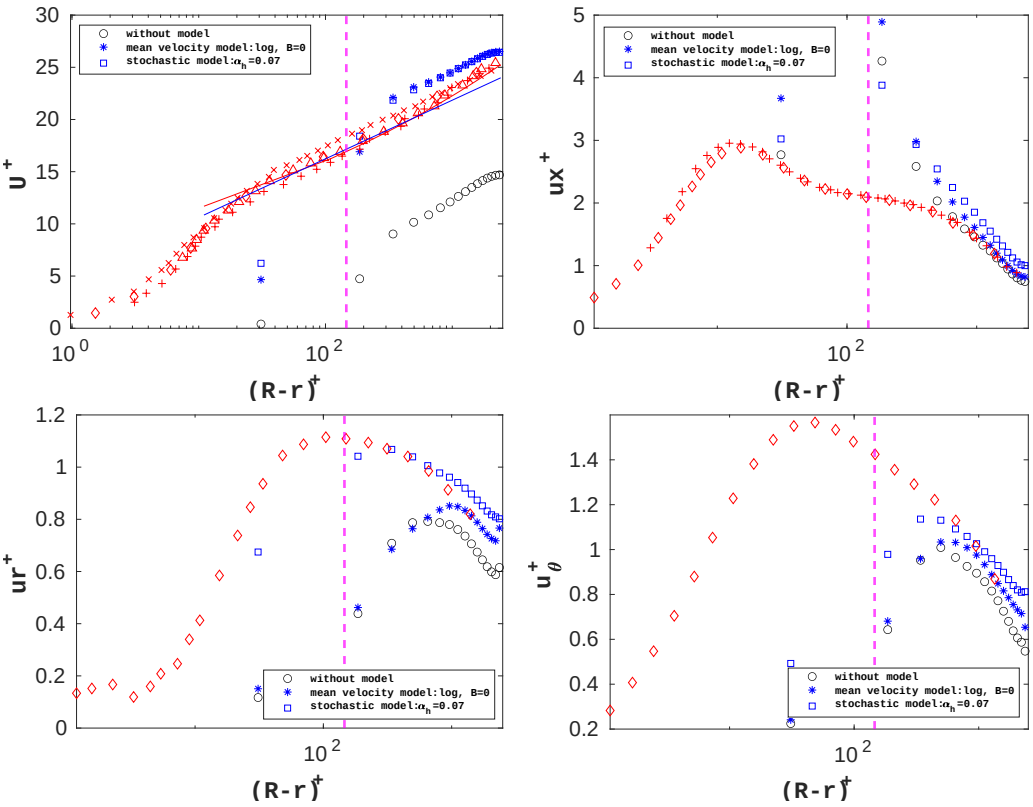

Figure 12: Comparison of the mean and RMS velocity, using a semi-logarithmic scale, profiles for $Re = 100,000$ obtained from the standard IBM without model (o) and with he mean velocity models ($*$) and the stochastic model ($\square$). Top left: mean velocity; top right: axial velocity RMS; bottom left: radial velocity RMS; bottom right: azimuthal velocity RMS. Red symbols stand for the reference studies: $\times$[14], $\wedge$, [11], $\diamond$[13], $+$[12] (see Table 1). Blue line: relation (28) for the "log law". Red line: relation (29) "power law". The vertical dashed line marks out the limit between the fluid and the IBM region ($\alpha_{IBM} > 0$).

This conclusion is confirmed when considering the total shear stress radial distribution. The contributions to the total shear are reported in Fig. 13 for simulations with no wall model (top-left), the mean velocity model (top-right) and the stochastic model (bottom-left). The comparison of the total shear stress obtained by these three approaches is also shown (bottom-right). The mean axial momentum equation can be integrated over r and divided by the fluid density ρ to get the following decomposition:

$$\frac{r}{R} = u_x u_r^+ - \nu \frac{\partial U^+}{\partial r} - \nu_t \frac{\partial U^+}{\partial r} + L_{xr}^+ - \nu_t' (\frac{\partial u_x}{\partial r} + \frac{\partial u_r}{\partial x})^+ \tag{39}$$

where $u_x u_r$ is the Reynolds stress contribution, $\nu \frac{\partial U}{\partial r}$ is the mean viscous shear contribution, $\nu_t \frac{\partial U}{\partial r}$ is the mean shear contribution resulting form the turbulent viscosity modeling, L_{xr} is the Leonard term and $\nu_t' (\frac{\partial u_x}{\partial r} + \frac{\partial u_r}{\partial x})$ is the mean shear stress due to the turbulent viscosity fluctuation which is usually negligible. We show in Fig. 13 the radial distribution of each of the above quantities normalized by u^{*^2} and we compare their sum (total normalized shear) to the expected linear function r/R according to equation 39. As observed all the approaches are able to reproduce the expected linear radial evolution in the pipe center. Close to the wall, the use of the stochastic model clearly improves the total shear stress balance. Note that the improvement is mainly due to the turbulent viscosity term that is dominating for such coarse resolution.

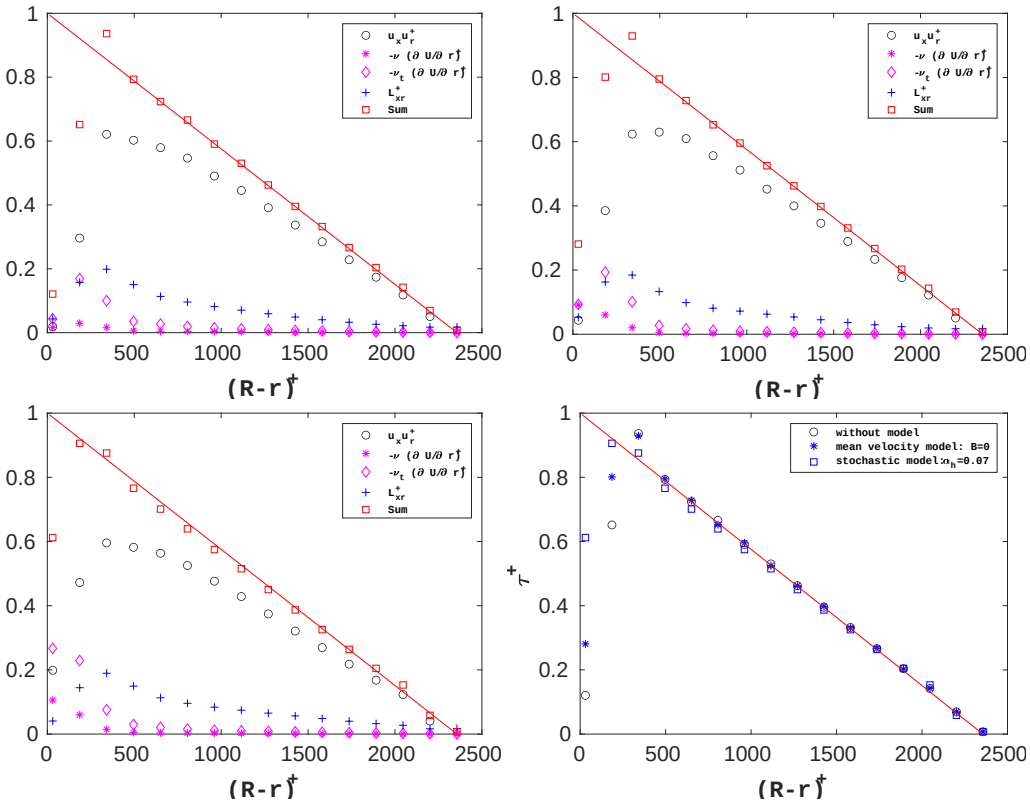

Figure 13: Comparison of the normalized shear between: no wall model (top-left), mean velocity model (top-right) and the stochastic model (bottom-left) for Re = 100,000 and mesh $m2$. Comparison between these three approaches (bottom-right). The red line represents the linear variation r/R for the expected total shear (left side of the equation 39).

4.3.2 Sensitivity of model parameters to grid resolution and Reynolds number

The previous analysis has been conducted for a selected Reynolds number $Re = 100,000$ and a given grid resolution (mesh $m2$). Each model has been tuned to provide the correct bulk velocity and optimized parameters have been proposed: $B = 0$, $A = 5.8$ and $\alpha_h = 0.07$ for the log law model, the power law model and the stochastic model, respectively. A similar investigation can be conducted for different Reynolds numbers and grid resolutions. The objective is now to discuss the effects of both the grid resolution and the pipe Reynolds number on the optimized values for B, A and α_h. For that purpose, numerical simulations are carried out for the three Reynolds numbers $Re = 50,000$, $100,000$ and $500,000$ and the three meshes $m1, m2$ and $m3$. For each case, each model is considered and the corresponding model parameter (B, A or α_h) is adjusted in order to obtain the correct bulk velocity (with a relative difference on E_U less than 1%), while imposing a constant value to the mean pressure drop as specified in section 4.
Figure 14 (left) reports the evolution of the optimized values of A and B as a function of the grid resolution for the three Reynolds numbers. Both A and B have to be increased when the mesh is getting coarser, because an underestimate of the bulk velocity is enhanced resulting in a stronger forcing required inside the IBM wall region. A linear evolution with the grid size is observed for both A and B. The starting point of the linear evolution for A (power law) needs to be adjusted for each Reynolds number while the linear fit of B (log law) is unchanged for the three different Reynolds numbers, outlining the relevance of using the log law modeling based on the analytical solution close to the wall. As shown in Fig. 14, the evolution of A can be simply described using the relation

$$A = 20.5\,\frac{\Delta}{R} + X(Re) \tag{40}$$

with the evolution of $X(Re)$ versus Re reported in Fig. 14 (right). The evolution of B can be described using the relation

$$B = 37.6\,\frac{\Delta}{R} - 2.23 \tag{41}$$

Note that while the value of the coefficient B becomes negative for sufficiently fine mesh, the IBM velocity $v_{s,x}$ for $r^+ > 11$ remains positive. Indeed, for consistency the IBM velocity needs to tend to 0 as the mesh is refined.

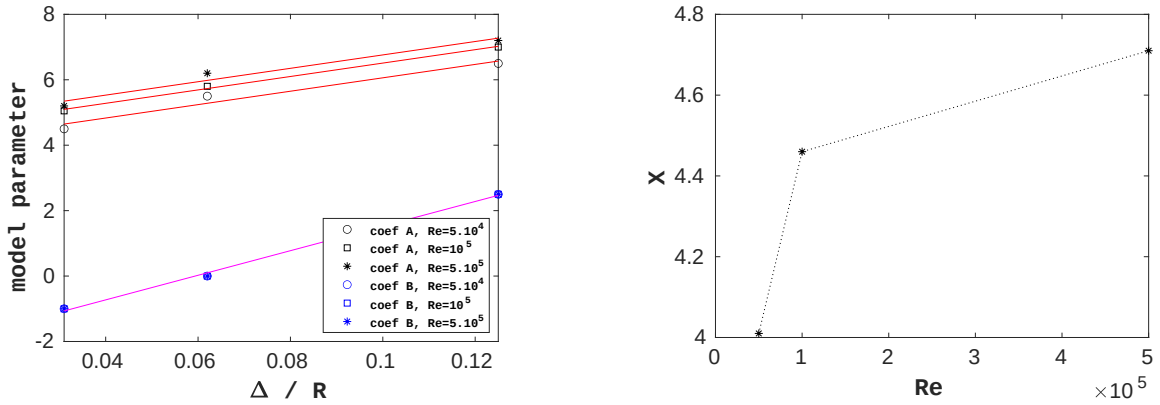

Figure 14: Optimal values for A and B as a function of the mesh resolution R/Δ for different Reynolds numbers Re (left). Lines stand for the linear fits 40 and 41. Evolution of $X(Re)$ (see relation 40) (right).

The variation of α_h (stochastic model) is reported in Fig. 15. α_h is found to decrease with the grid spacing. In fact, as the mesh gets coarser, the simulated bulk velocity is decreased and wall friction has to be reduced. This can be directly controlled with a reduction of the magnitude of the fluctuations imposed inside the IBM wall region. However, the same order of magnitude $\alpha_h = O(0.1)$ is observed for the different Reynolds numbers and grid resolutions considered. A first rough estimate of the evolution of α_h can be described with

$$\alpha_h = 2.5\,10^{-4}\left(\frac{\Delta}{R}\right)^{-2} \tag{42}$$

for the range of Reynolds number we considered.

The stochastic model is based on an instantaneous log law description ($B = 5$ being imposed) of the velocity inside the IBM wall thickness (see relation (31)). As shown above changing B when using the log model only and α_h when using the stochastic forcing (B being set fixed) have both a clear impact on the bulk velocity. A better optimization of the combination of B and α_h in the stochastic model may certainly provide a better description of the fluctuation level and peak location.

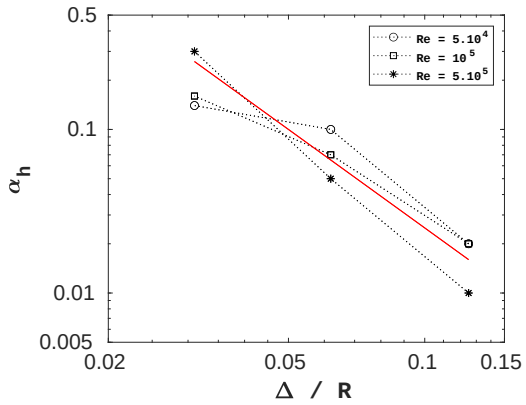

Figure 15: Optimal α_h as a function of the mesh resolution Δ/R for different Reynolds numbers Re. – relation (42)

4.3.3 Flow streaks

The turbulent flow fields obtained with the different approaches are now compared. The Reynolds number is $Re = 100,000$, the mesh is $m2$ and numerical simulations with the optimized parameters ($B = 0$, $A = 5.8$ and $\alpha_h = 0.07$) are compared to the basic IBM wall forcing. Figure 16 represents an instantaneous snapshot of the axial fluctuations u'_x normalized by the bulk velocity $< U >$ at a section along the pipe axis. The fluctuations seem to have almost the same structures in the four cases. No noticeable difference can be observed and a zoom close to the wall is proposed in Fig. 17 where $u'_x/ < U >$ is plotted at a distance of 100 ℓ^* away from the wall.

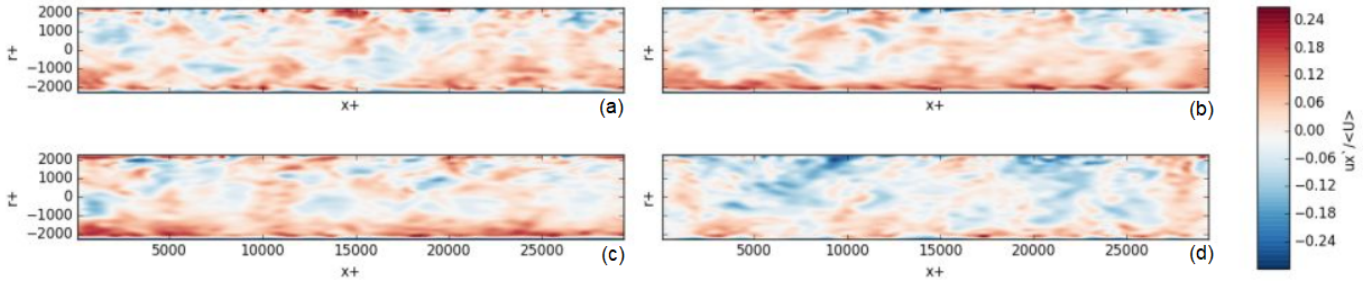

Figure 16: Normalized instantaneous axial fluctuations $u'_x/ < U >$. (a) basic IBM wall forcing, (b) mean velocity model: log law, (c) mean velocity model: power law, (d) stochastic model.

Figure 17 clearly points out a difference in the streaks organization close to the wall. As shown, basic IBM forcing, log law and power law models provide similar fluctuation structures close to the wall. The streaks in those cases are somehow damped yielding to a reduced turbulence intensity. On the opposite, the stochastic model enhances the flow fluctuations and typical high-speed and low-speed streaks are observed in Fig. 17 (d).

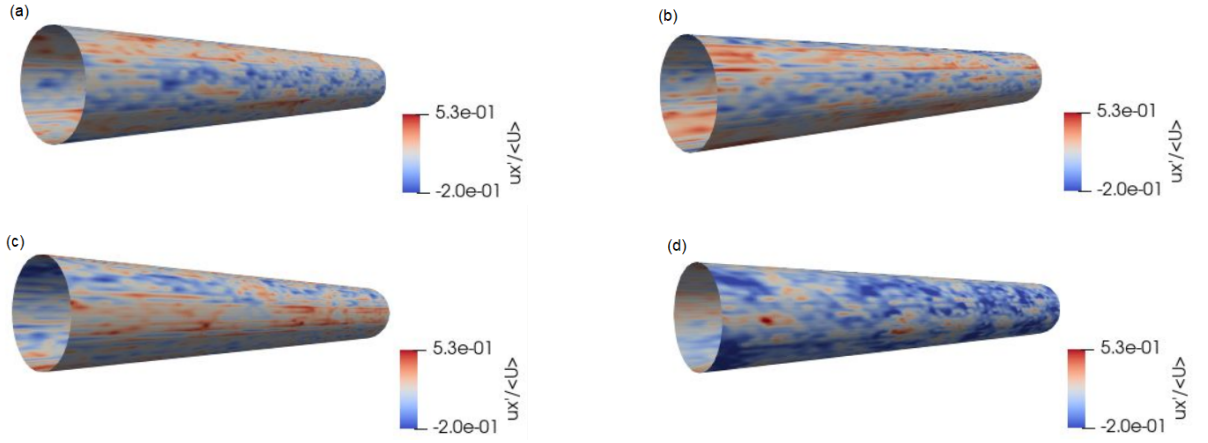

Figure 17: Streaks observation. Normalized instantaneous axial fluctuations $u'_x/ < U >$ at the distance $100\ell^*$ away from the wall. (a) Basic IBM wall forcing, (b) mean velocity model: log law, (c) mean velocity model: power law, (d) stochastic model.

We also compare the impact on the LES resolution of the different IBM wall models. For that purpose the total viscosity $\nu_{total} = \nu + \nu_T$ is considered. Figure 18 reports an instantaneous field of ν_{total} made dimensionless by the fluid cinematic viscosity ν in a pipe section. As shown, the intensity of ν_t is enhanced when using the stochastic model. From a LES modeling point of view, this can be explained by the induced effect of the fluctuations on the strain rate tensor and the local Smagorinsky coefficient C used to calculate the sub-grid viscosity ν_T.

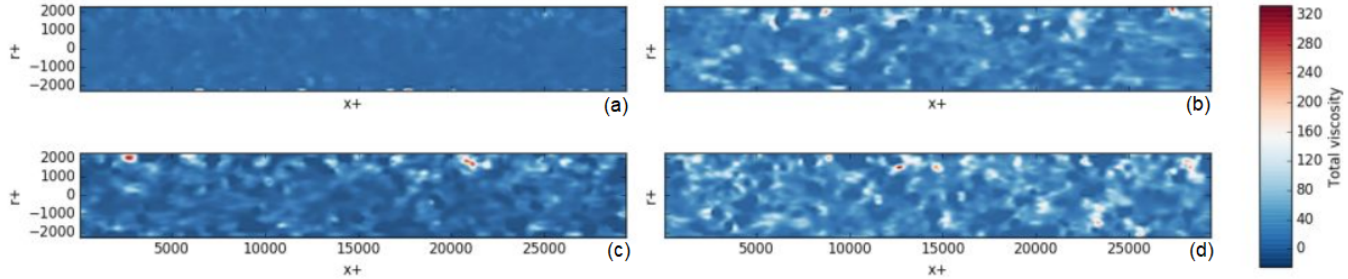

Figure 18: Normalized total viscosity ν_{total}/ν: (a) basic IBM wall forcing, (b) mean velocity model: log law, (c) mean velocity model: power law, (d) stochastic model.

4.3.4 Effect of the models on the pressure field

We finally discuss the effect of the different models on the pressure. For that, we plot the mean and RMS values of the pressure for $Re = 50,000$ and compare them to a previous DNS performed at $Re = 37,700$ [44]. Figure 19 represents the pressure normalized by $\rho u^{*2}/2$ as a function of the distance from the wall. The mean pressure profile is reported by considering the mean wall pressure as the reference pressure. We can see in the figure that our IBM-LES simulations without and with the mean velocity model give comparable evolution to the reference DNS for both the mean and RMS profiles of the pressure. However, the stochastic model with the optimal α_h as determined previously with the criteria to reproduce the correct bulk velocity introduces higher pressure fluctuations. Figure 20 shows the normalized instantaneous pressure field for each case at the distance $100l^*$ away from the wall. A different distribution and higher extreme values for the pressure are observed with the stochastic model, this effect being enhanced when increasing the value of α_h. This behavior is attributed to the response of the Poisson solver because the

imposed local velocity in the IBM forcing is not divergence free. Increasing α_h, the stochastic forcing both in time and in space leads the solver to produce large pressure fluctuations.

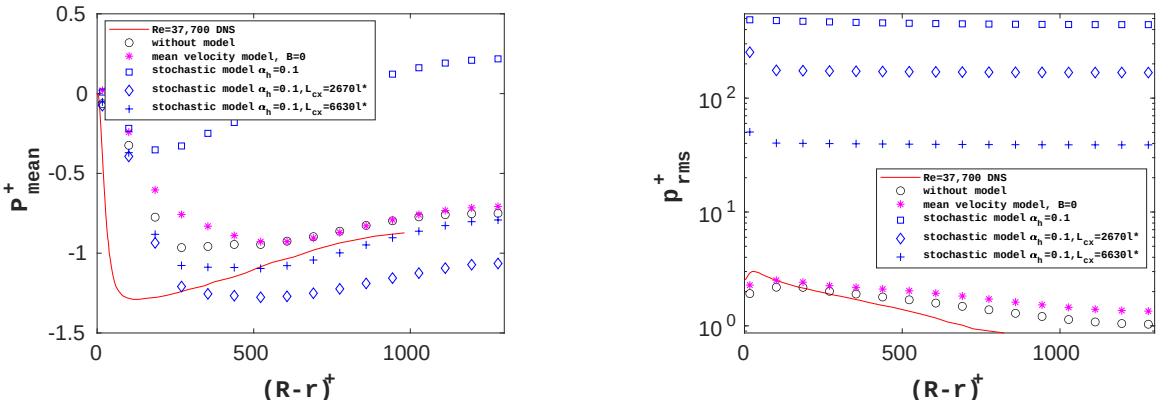

Figure 19: Pressure statistics for $Re = 50,000$ compared to the reference DNS [44] at $Re = 37,700$. (left) mean profile, (right) RMS profile.

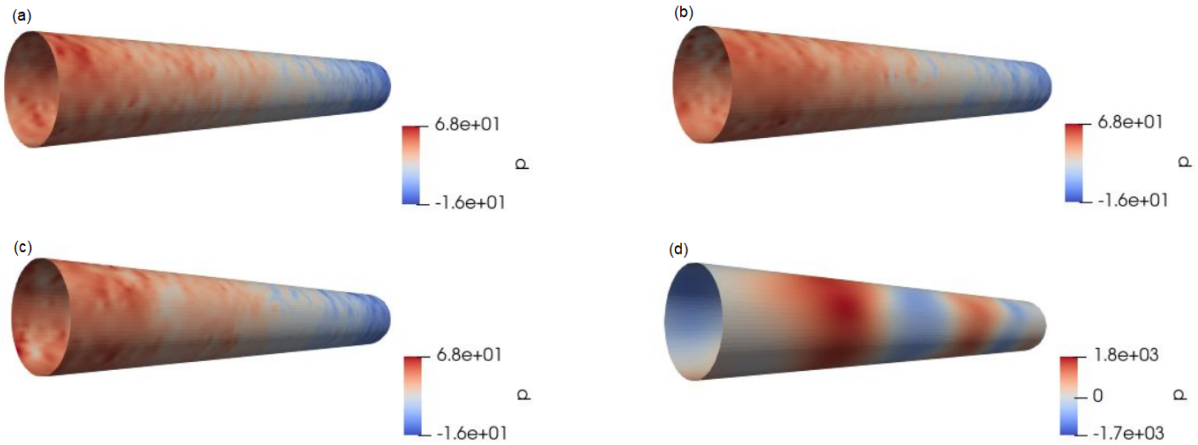

Figure 20: Normalized instantaneous pressure field for $Re = 50,000$ at $100l^*$ away from the wall. (a) Basic IBM wall forcing, (b) mean velocity model: log law, (c) mean velocity model: power law, (d) stochastic model. Note that the pressure range has been adjusted in (d).

Coming back to our stochastic model, two parameters are controlling the imposed characteristic length and time of the model, namely, T_c and L_{cx}. Simulations (not reported here) considering a fixed α_h have revealed that acting only on T_c does not influence the pressure response, while using higher length correlation L_{cx}, the instantaneous pressure field, the mean pressure and the RMS values are improved compared to the reference case. This is illustrated via the pressure statistics in Fig. 19 and the pressure fields in Fig. 21 that compare the normalized instantaneous pressure field when taking $L_{cx} = 2570l^*$ and $L_{cx} = 6630l^*$ instead of $L_{cx} = 1000l^*$ used for the simulation reported in Fig. 20.d. However the bulk velocity is then overestimated and the error on the bulk velocity surpasses 1%. Increasing the correlation length L_{cx} decreases the pressure fluctuations while increasing the bulk velocity, and if we want to recover (i.e. decrease) the mean velocity, we have to increase α_h which directly induces again the increase of the pressure fluctuations level. Finding the couple (α_h, L_{cx}) which can reproduce both the correct bulk velocity and the pressure fluctuation level can be performed but it needs some iterations, reducing the interest of the modeling compared to the use of a mean velocity. This is the reason why we consider that a future development of this work consists of developing a stochastic divergence-free IBM forcing model while keeping α_h as the only adjustable model parameter.

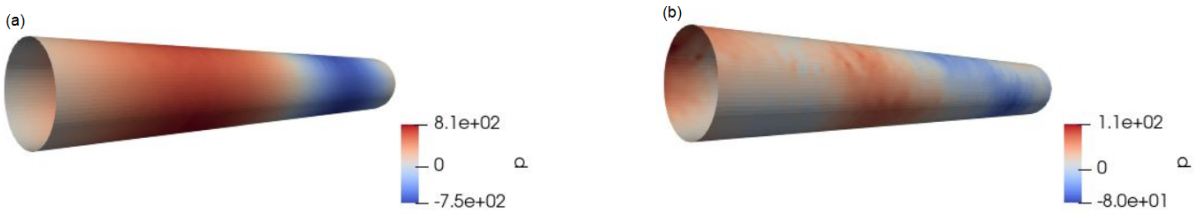

Figure 21: Normalized instantaneous pressure for $Re = 50,000$ at $100l^*$ away from the wall using the stochastic model $\alpha_h = 0.1$. (a) $L_{cx} = 2570l^*$, (b) $L_{cx} = 6630l^*$, to be compared to Fig.20.d where $L_{cx} = 1000l^*$.

5 Conclusion

A hybrid IBM-LES method has been presented addressing the challenge to simulate high-Reynolds number pipe flows on coarse Cartesian meshes. Firstly, the IBM method is used to simulate a laminar pipe flow and numerical results demonstrate a second order convergence to the exact solution. By introducing the correct solid velocity condition in the forcing term across the IBM wall thickness, the convergence is remarkably improved and the method underlines its efficiency. Then, turbulent pipe flows of Reynolds numbers in the range 50,000 to 500,000 are considered coupling the IBM method with the LES solver. As expected, the use of a coarse grid resolution does not allow to reproduce both the mean bulk velocity and the fluctuations. Extending the IBM wall modeling introduced for the simulation of the laminar pipe flow, an IBM wall forcing scheme is proposed based on the classical turbulent wall laws, namely the log-law and the power-law, able to predict the mean velocity profile. We show that adjusting the control parameters of these two models allows recovering the correct bulk velocity and mean velocity profiles. With the aim of improving the fluctuations and spatial distribution of streaks inside the pipe, the log law modeling is coupled to a stochastic wall model to generate an unsteady and non-uniform forcing within the IBM wall thickness. The level of velocity fluctuations is then improved close to the wall approaching the reference data. The effect of both the Reynolds number and grid resolution are then discussed and empiric correlations for the model parameters are established. Discussing the response of the pressure to the stochastic forcing, we conclude that further development of the stochastic modeling for the velocity in the IBM wall region are required, in particular a divergence-free stochastic velocity forcing should make the prediction of the velocity and pressure RMS in the near-wall region more accurate. The main interest of the hybrid IBM-LES presented here is to demonstrate that simulations coupling LES and IBM can be performed for highly turbulent pipe flows with a coarse Cartesian resolution through a wall model. This is of great interest for the simulation of high Reynolds number flows not only in simple geometries but also in complex geometries that can be described in the framework of IBM approach thanks to the use of an appropriate IBM function to define the domain. Indeed, owing to the universality of turbulent near-wall flows, we believe that this method is much more general. Specifically, the approach should be applicable to all fully developed turbulent flows (e.g. plan channel flows, boundary layers) without significant modifications. Concerning flows in more complex geometries, it is likely that the model should be enriched to account for non-equilibrium effects such as adverse pressure gradients, 3D effects, boundary layer detachments ... However the present work is a first step towards building a more general approach. Such generalization to more complex flows is currently being investigated and we recently considered the flows around an axial swirler [20, 21].

Acknowledgments

This work is done within the TOMOCON project which has received funding from the European Union's Horizon 2020 research and innovation program under the Marie Sklodowska Curie grant agreement No 764902. The numerical simulations were performed using high-performance computing resources from CALMIP at the University of Toulouse under the project (P0910).

References

[1] Pope S. B. *Turbulent flows*. Cambridge University Press, 2000.

[2] Sagaut P. *Large eddy simulation for incompressible flows: an introduction*. Springer Verlag, 2nd edition, 2002.

[3] H. Choi and P. Moin. Grid-point requirements for large eddy simulation: Chapman's estimates revisited. *Physics of Fluids*, 2012.

[4] Peskin C.S. Numerical analysis of blood flow in the heart. *J. Comput. Phys*, 1977.

[5] J.H. Seo and R. Mittal. A sharp-interface immersed boundary method with improved mass conservation and reduced spurious pressure oscillations. *Journal of Computational Physics*, 2011.

[6] Tessicini F., Iaccarino G., Fatica M., Wang M., and Verzicco R. Wall modeling for large-eddy simulation using an immersed boundary method. *Standford University. Annual Research Briefs*, 2002.

[7] Cristallo A. and Verzicco R. Combined immersed boundary/large-eddy-simulations of incompressible three dimensional complex flows. *Flow Turbulence Combust*, 2006.

[8] Roman F., Armenio V., and Frohlich J. A simple wall-layer model for large eddy simulation with immersed boundary method. *Physics of Fluids*, 2009.

[9] Ma M., Huang W., and Xu C. A dynamic wall model for large eddy simulation of turbulent flow over complex/ moving boundaries based on the immersed boundary method. *Physics of Fluids*, 2019.

[10] Laufer J. The structure of turbulence in fully developed pipe flow. Technical report, NACA-TR-1174, 1953.

[11] Zagarola M.V. and Smits A.J. Mean-flow scaling of turbulent pipe flow. *J. Fluid Mech*, 1998.

[12] Hultmark M., Vallikivi M., Bailey S.C.C., and Smits S. Logarithmic scaling of turbulence in smooth-hand rough-wall pipe flow. *J. Fluid Mech*, 2013.

[13] Chin C., Monty J.P., and Ooi A. Reynolds number effects in dns of pipe flow and comparison with channels and boundary layers. *International Journal of Heat and Fluid Flow*, 2014.

[14] Vijiapurapu S. and Cui J. Performance of turbulence models for flows through rough pipes. *Applied Mathematical Modelling*, 2010.

[15] Calmet I. and Magnaudet J. Large eddy simulation of high schmidt number mass transfer in a turbulent channel flow. *Physics of Fluids*, 1997.

[16] Legendre D. and Magnaudet J. The lift force on a spherical body in a viscous linear shear flow. *J. Fluid Mech.*, 1998.

[17] Bigot B., Bonometti T., Thual O., and Lacaze L. A simple immersed boundary method for solid fluid interaction in constant and stratified density flows. *J. Computers and fluids*, 2014.

[18] Yuki Y., Takeuchi S., and Kajishima T. Efficient immersed boundary method for strong interaction problem of arbitrary shape object with the self-induced flow. *Journal of Fluid Science and Technology*, 2007.

[19] Merle A., Legendre D., and Magnaudet J. Forces on a high reynolds number spherical bubble in a turbulent flow. *J. Fluid Mech*, 2005.

[20] Atmani H., Zamansky R., Climent E., and Legendre D. Cfd approach to simulate two phase flow inline-separator coupling ibm, les, lagrangian tracking and vof methods. In *SINTEF Proceedings 6*, 2020.

[21] Garcia M.M., Sahovic B., Sattar M.A., Atmani H., Schleicher E., Hampel U., Babout L., Legendre D., and Portela L.M. Control of a gas-liquid inline swirl separator based on tomographic measurements. *IFAC-PapersOnLine*, pages 53/2, 11483–11490, 2020.

[22] Canuto C., Hussaini M. Y., Quarteroni A., and Zang T. A. Spectral methods for fluid dynamics. *Springer-Verlag, Berlin*, 1988.

[23] Rai M.M. and Moin P. Direct simulations of turbulent ?ow using ?nite difference schemes. *J. Comput. Phys.*, 1991.

[24] Cheng W. and Samtaney R. Power law versus log law in wall bounded turbulence: A large eddy simulation perspective. *Physics of Fluids*, 2014.

[25] Karman Th. V. Mechanical similitude and turbulence. *Tech. Mem. NACA*, 1931.

[26] Werner H. and H. Wengle. *Large-eddy simulation of turbulent flow over and around a cube in a plate channel*. Turbulent Shear Flows, Springer-Verlag, editor, Munich, Germany, 1993.

[27] Jiménez J. and Pinelli A. The autonomous cycle of near-wall turbulence. *Journal of Fluid Mechanics*, 389:335–359, 1999.

[28] Smits A.J., B. J. McKeo, and Marusic I. High-Reynolds Number Wall Turbulence. *Annual Review of Fluid Mechanics*, 43:353–375, 2011.

[29] Pan C. and Kwon Y. Extremely high wall-shear stress events in a turbulent boundary layer. *J. Phys.: Conf. Ser.*, 1001:012004, 2018.

[30] N. Hutchin, Monty J. P., Ganapathisubramani B., H. C. H. Ng, and Marusic I. Three-dimensional conditional structure of a high-reynolds-number turbulent boundary layer. *Journal of Fluid Mechanics*, 673:255–285, 2011.

[31] Gomit G., de Kat R., and Ganapathisubramani B. Structure of high and low shear-stress events in a turbulent boundary layer. *Physical Review Fluids*, 3(1), jan 2018.

[32] Townsend A. A. Equilibrium layers and wall-turbulence. *Journal of Fluid Mechanics*, 11:97–120, 1961.

[33] Perry A. E., S. Henbes, and Chong M. S. A theoretical and experimental study of wall turbulence. *Journal of Fluid Mechanics*, 165:163–199, 1986.

[34] Maniero R., Climent E., and Bacchin P. Adhesion and detachment fluxes of micro-particles from a permeable wall under turbulent flow conditions. *Chem. Eng. Sciences*, 2012.

[35] Sheng J., Malkiel E., and Katz J. Buffer layer structures associated with extreme wall stress events in a smooth wall turbulent boundary layer. *J. Fluid Mech.*, 2009.

[36] Alfredsson P. H., Johansson A. V., Haritonidis J. H., and Eckelmann H. The fluctuating wall-shear stress and the velocity field in the viscous sublayer. *Physics of Fluids*, 31(5):1026, 1988.

[37] Smith C.R and Metsler S.P. The characteristics of low speed streaks in the near wall region of turbulent boundary layer. *J. Fluid Mech*, 1983.

[38] Chernyshenko S.I. and Baig M.F. The mechanism of streak formation in near wall turbulence. *J. Fluid Mech*, 2005.

[39] Wallace J.M. Space-time correlations in turbulent flow: review. *Theoretical and applied mechanics letters*, 2014.

[40] He G., Jin G., and Yang Y. Space-time correlations and dynamic coupling in turbulent flows. *Annu. Rev. Fluid Mech*, 2017.

[41] Monty J. P. and Chong M. S. Turbulent channel flow: comparison of streamwise velocity data from experiments and direct numerical simulation. *Journal of Fluid Mechanics*, 633(-1):461–474, 2009.

[42] Del Álamo J. and Jiménez J. Estimation of turbulent convection velocities and corrections to taylor's approximation. *Journal of Fluid Mechanics*, 640:5–26, 2009.

[43] Kreplin H and Eckelmann H. Propagation of perturbations in the viscous sublayer and adjacent wall region. *Journal of Fluid Mechanics*, 95(2):305–322, 1979.

[44] El Khoury G., Schatther P., Noorani A., Fischer P., Geert Brethouwer G., and Johansson A. Direct numerical simulation of turbulent pipe flow at moderately high reynolds numbers. *Flow Turbulence Combust*, 2013.